Molecular-dynamics simulation of MgO surfaces in liquid water using a shell-model potential for water

N. H. de Leeuw* and S. C. Parker†
School of Chemistry, University of Bath, Claverton Down, Bath BA2 7AY, United Kingdom
(Received 18 May 1998)

A shell-model water potential, derived to be compatible with existing potential models for inorganic solids, is introduced. It reproduces experimental data of the water monomer and dimer such as structure, dipole moment, and binding energy. Properties of liquid water, especially ordering and energetics, are in adequate agreement with experiment. The polarizable water potential model is used to model the interaction of liquid water with MgO surfaces. Adsorption of the first monolayer to the surfaces is shown to disrupt ordering in the next layers, leading to decreased water density near the solid surface. [S0163-1829(98)07440-2]

I. INTRODUCTION

Due to its omnipresence and unique structure, water in both liquid and solid form has been the subject of wide-ranging research, both experimental (e.g., Refs. 1–7) and theoretical (e.g., Refs. 4 and 8–13), for example the studies of both liquid water and ice I_h by x-ray scattering[14] and phonon calculations.[15] In solid form water exists as 13 different ice structures, including a vitreous form and two relatively unknown phases. The most common ice is hexagonal ice *I*, which occurs at atmospheric pressure up to 273 K.[16] The common feature of all ice phases is the tetrahedral arrangement of hydrogen atoms surrounding each oxygen atom, where two hydrogen atoms are bonded to the oxygen, while the other two form hydrogen bonds to the lone electron pairs. This arrangement leads to considerable disorder in the ice phases, notably in ice I_h which has ideal tetrahedral coordination. However, even in the denser ice phases, where the coordination is not perfectly tetrahedral, at high temperatures the gain in configurational entropy accompanying disorder of the hydrogen atoms outweighs the energy expended by some orientations departing from the ideal angle.[17] In liquid water, although destabilized by entropy, this tetrahedral arrangement remains partially intact.[18]

One of the aims of this work was to develop a reliable and consistent model for the interaction of water with solid surfaces. Although there is a wealth of different water potentials available,[11,19–28] from simple SPC models to point-polarizable TIP models,[21] to our knowledge no shell-model potential is as yet available for the modeling of polarizable water molecules. In this potential model the polarizability of the oxygen ion is included by the shell model of Dick and Overhauser,[29] and the shell model potential can thus be used for simulations of the interactions of water molecules with the surfaces of ionic solids for which the same type of potential models are currently widely available.

The interaction of water molecules with the surfaces of a variety of materials, both metals and inorganic solids, has been the subject of much research (e.g., Refs. 30–35). One material which has been studied extensively is the ceramic oxide MgO. Its relatively simple structure, i.e., face-centered-cubic with six coordinate oxygens and cations, and its importance both as a support for metal catalysts and high-temperature superconductors[36] and as a catalyst in its own right,[37,38] make it an attractive model system. As a consequence, the structure and hydration of MgO surfaces has been frequently investigated, both experimentally[37,39–44] and theoretically.[35,36,45–51] MgO would thus seem an appropriate system to test the applicability of our polarizable water potential model.

II. THEORETICAL METHODS

Atomistic simulations are based on the Born model of solids,[52] which assumes that the ions interact via long-range electrostatic forces and short-range forces which can be described using simple analytical functions. The components of the short-range forces include both the repulsions and the van der Waals attractions between neighboring electron charge clouds. The Coulombic interactions are summed using the Ewald method[53] for three-dimensional periodic systems, such as bulk crystals, or the Parry method[54,55] in the case of two-dimensional periodicity, e.g., surfaces. The potential model of a system is the set of charges and functional parameters needed to describe all interactions between the participating species.

A large number of potential models available for solids, both purely ionic and those including molecular ions such as the carbonate anion, include the polarizability of the ions in the system via the shell model of Dick and Overhauser.[29] This shell model describes the ion in a simple mechanical way by a shell of zero mass representing the electronic charge cloud connected to a core containing all the ion's mass. The total charge of the ion is the sum of the charges of core and shell. The position of the core represents the position of the ion in the crystal lattice, but the position of the shell has no significance.[56] The shell and core are connected by a harmonic spring with force constant *k*:

$$\Phi_i(r_i) = \tfrac{1}{2} k_i r_i^2, \tag{1}$$

where r_i is the distance between the centres of core and shell. The polarizability α of the free ion is then given as

$$\alpha_i = \frac{Y^2}{4\pi\varepsilon_0 k_i}, \tag{2}$$

where Y is the charge of the shell. The polarization of an ion is described in terms of the displacement of its shell relative to the core. Unlike point-polarizable models which have a fixed polarizability, the shell model allows the polarizability to vary with environment. It allows for coupling between the polarizability of the ion and its short-range interactions, which is required to model dynamical properties, for example lattice vibrations reliably.[57] The short-range forces are assumed to act between the shells, while the Coulombic forces act between all shells and cores except between the core and shell of the same ion. Although the shell model is relatively simple, it has been very successful in modeling a variety of properties and, as such, in addition to its wide application in available potential models, we sought to develop a potential model for the water molecule which included polarizability of the oxygen ion via the shell model of Dick and Overhauser.[29] This would then be fully compatible with the potential models used for inorganic solids, and hence could be used to model the interaction of water with solid surfaces. In Sec. II A we describe the derivation of the potential parameters which make up the potential model, after which we discuss its competence in reproducing experimental water properties.

A. Derivation of the water potential

The potential parameters for the water molecule were empirically fitted to reproduce the experimental dipole moment, OH bond length and HOH angle of the water monomer, and the structure of the water dimer and infrared data. The potential model was subsequently used to calculate the self-diffusion coefficient, radial distribution functions, and energy of evaporation of liquid water.

The atoms making up the molecule were given fractional charges, $+0.4e$ for the hydrogen atom, in line with the compatible hydroxide potential model developed by Baram and Parker[58] and many earlier water potential models,[21,24,25] and $-0.8e$ for the oxygen atom, which is the sum of the charges of core of $+1.250e$ and shell of $-2.050e$. All potential interactions involving oxygen atoms act between their shells. The OH bond is modeled by a Morse potential

$$\Phi_{ij}(r_{ij}) = D(1 - e^{[-\alpha(r_{ij}-r_0)]})^2 - D, \tag{3}$$

where D is the dissociation energy of the bond, r_{ij} is the interatomic separation, and r_0 is the equilibrium separation. α is a variable which can be determined by spectroscopic data and was fitted to the experimental infrared frequencies using the program GULP.[59] A bond-bending term was introduced to reproduce the directionality of the covalent bonds with the experimental HOH angle of 104.5°,

$$\Phi_{ijk}(r_{ijk}) = \tfrac{1}{2} k_{ijk}(\theta_{ijk} - \theta_0)^2, \tag{4}$$

which is a simple harmonic about the equilibrium bond angle, where k_{ijk} is the force constant and $(\theta_{ijk} - \theta_0)$ is the deviation of the bond from the equilibrium angle. In addition to these short-range interactions, we endeavored to model the effect the oxygen atoms' electron lone pairs have on the positions of the hydrogen atoms and hence on the HOH angle. In an attempt to include the steric effect of the electron lone pairs, we partially removed the electrostatic interactions between the two hydrogen atoms and those between hydrogen and oxygen atoms in the water molecule, making the hydrogen atoms less repulsive, much as electrostatic interactions within organic molecules are routinely removed in potential models for biological applications.

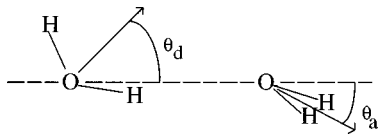

FIG. 1. Configuration of the water dimer (Refs. 1 and 23).

The intermolecular parameters for the water molecules were fitted to the structure of the water dimer which is shown in Fig. 1.[1] θ_d refers to the angle in the dimer between the O-O vector and the C_2 axis of the water molecule donating its one hydrogen atom for hydrogen bonding to the oxygen molecule of the acceptor molecule. θ_a refers to the angle between the O-O vector and the C_2 axis of the acceptor molecule. The short-range interactions between the oxygen shells of the water molecules are described by a Lennard-Jones potential

$$\Phi_{ij}(r_{ij}) = \frac{A}{r_{ij}^{12}} - \frac{B}{r_{ij}^{6}}, \tag{5}$$

where A and B are variable parameters. This type of potential expression is often used for modeling oxygen-oxygen interactions in water potential models, such as the SPC and TIP4P models.[21,25] The intermolecular interactions between hydrogen cores and oxygen shells are given by a Buckingham potential

$$\Phi_{ij}(r_{ij}) = A_{ij} e^{-(r_{ij}/\rho_{ij})} - \frac{C_{ij}}{r_{ij}^{6}}, \tag{6}$$

where the parameters A_{ij} and ρ_{ij} are often thought to represent the size and hardness of the atoms, respectively, although in this work the Buckingham potentials are effective pair potentials, and hence the two parameters are not independent. The last term is meant to represent the dispersive forces.

The potential model used for simulating the MgO crystal is that of Lewis and Catlow,[60] while the interactions between the water molecules and the solid surface were fitted by ourselves. Following the approach by Schroder *et al.*,[61] the cation-oxygen Buckingham potential of the MgO crystal needs to be modified for the Mg-O_{water} interaction to compensate for the reduction in electrostatic interaction due to the latter's fractional charge. The C parameter of the Buckingham potential function between lattice oxygen atoms was also modified for interactions between lattice oxygen atoms and water oxygen atoms assuming this represents London dispersion forces. All potential parameters used in this work are listed in Table I.

B. Molecular-dynamics simulations

The computer code used for the molecular dynamics simulations was DL_POLY 2.6.[62] To obtain the necessary data

TABLE I. Potential parameters used in this work.

Ion	Charges (e) Core	Shell	Core-shell interaction (eV Å^{-2})
Mg^{2+}	2.00+		
$H^{0.4+}$	0.40+		
Oxide oxygen O^{2-}	1.00+	3.00−	54.80
Water oxygen $O^{0.8-}$	1.25+	2.05−	209.45

Buckingham potential

Ion pair	A (eV)	ρ (Å)	C (eV Å^6)
$Mg^{2+}-O^{2-}$	1428.50	0.294 53	0
$Mg^{2+}-O^{0.8-}$	490.00	0.294 53	0
$O^{2-}-O^{2-}$	22764.00	0.149 00	27.88
$O^{2}-O^{0.8-}$	22764.00	0.149 00	28.92
$H^{0.4+}-O^{0.8-}$	396.27	0.250 00	10.0
$H^{0.4+}-O^{2-}$	396.27	0.250 00	0.0

Lennard-Jones potential

	A (eV Å^{12})	B (eV Å^6)
$O^{0.8-}-O^{0.8-}$	39344.98	42.15

Morse potential

	D (eV)	α (Å^{-1})	r_0 (Å)
$H^{0.4-}-O^{0.8-}$	6.203 713	2.220 03	0.923 76

Three-body potential

	k (eV rad^{-2})	Θ_0
$H^{0.4+}-O^{0.8-}{}_{\text{shell}}-H^{0.4+}$	4.199 78	108.69

Coulombic subtraction (%)

$H^{0.4+}-O^{0.8-}$	50
$H^{0.4+}-H^{0.4+}$	50

on bulk liquid water, we simulated a box containing 256 water molecules at a temperature of 300 K. The simulation conditions were initially set at the experimental density of $\rho = 1.0$ g/cm^3 and performed using NVE and NVT (constant number of particles, constant volume, and constant energy or temperature) ensembles. When those were successful, equilibration and finally data collection were run at NPT (constant number of particles, constant pressure, and constant temperature). In the DL_POLY code the integration algorithms are based around the Verlet leap-frog scheme,[63] and we used the Nosé-Hoover algorithm[64,65] for the thermostat, as this algorithm generates trajectories in both NVT and NPT ensembles, thus keeping our simulations consistent. The Nosé-Hoover parameters were set at 0.5 for both the thermostat and barostat relaxation times (ps).

There are two ways of treating the shells which are essentially massless; either performing an energy minimization of shells only at each time step[66] or the approach used by DL_POLY, which is to assign a small mass to the shells.[67,68] In this case for the oxygen shell we chose 0.2 a.u., which is small compared to the mass of the hydrogen atom of 1.0 a.u. This ensured that there would be no exchange of energy between vibrations of oxygen core and shell with oxygen and hydrogen vibrations. Figure 2 shows a diagram of the phonon density of states for ice VII, from which it is clear that there is no overlap between OH frequencies at around 3700 cm^{-1} and oxygen core-shell vibrational frequencies at around 17 000 cm^{-1}, and we may thus be confident that there will be no exchange of energy between the hydrogen ions and the shells in our molecular-dynamics (MD) simulation. However, due to the small shell mass we needed to run the MD simulation with a small time step of 0.2 fs in order to keep the system stable. With this time step we obtained data at constant pressure and temperature for a period of 100 ps.

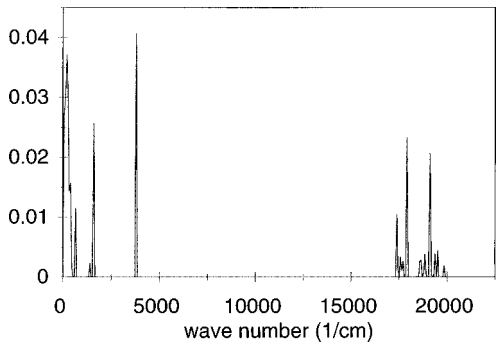

FIG. 2. Phonon density of states for ice VII with the shell model. The first group of peaks corresponds to acoustic and low-lying optic modes, the second group is due to H-O-H bending, and the third group is the O-H stretching mode. The last group, between 17 000 and 20 000 cm^{-1}, is due to oxygen core-shell vibrations.

The MgO surfaces were simulated as a repeating unit cell of MgO slab and void, and this system consisting of the pure surface *in vacuo* was run under NVT conditions. The void was then filled with NPT equilibrated bulk water, and the entire system of MgO slab and surrounding liquid water was simulated under NPT conditions. In addition, NVT simulations of the MgO slabs with lower-density water were also performed to investigate any differences in energetics due to the two different water densities.

III. RESULTS AND DISCUSSION

The water potential model derived above was fitted to the structural properties of the water monomer and dimer and infrared-absorption bands[69] of the water molecule. In order to assess how well these properties are reproduced using the program PARAPOCS,[70] we have listed the calculated and experimental data in Table II, from which it is clear that the experimental structure, dipole moment, and vibrational properties of the water monomer are accurately reproduced, which is as expected as they were used for fitting the potential model. The binding energy of the dimer and the oxygen-oxygen distance also agree very well with the experimental data, although θ_a, the angle between the O-O vector and the hydrogen acceptor molecule, is too small in common with other water potentials,[18,21,23] which makes the dimer rather flat. This may be due to the absence of a potential function describing directional hydrogen bonding between water molecules, as is found in ice.[71]

The properties calculated from the MD simulation were radial distribution functions, average energy, density, specific-heat capacity, compressibility, and the self-diffusion coefficient which can be obtained from the mean square deviation of the molecules.[72] The self-diffusion coefficient was

TABLE II. Experimental properties of water monomer and dimer which, apart from the binding energy, were used for fitting the potential parameters, and the resulting calculated values and E_{binding}.

H_2O	Properties	Calculated	Experimental
Monomer	r(OH)/Å	0.98	0.96[a]
	θ (HOH)	104.5°	104.5°[a]
	Dipole/D	1.86	1.85[a]
	ν/cm^{-1}	1581.95	1594.59[b]
	ν/cm^{-1}	3624.56	3656.65[b]
	ν/cm^{-1}	3783.00	3755.79[b]
Dimer	r(O-O)/Å	2.97	2.98[c,d,e]
	θ_α	30.1°	57±10°[c,d]
	θ_d	48.5°	51±10°[c,d]
	E_{binding}/eV	−0.21	−0.23[d]

[a]Reference 26.
[b]Reference 69.
[c]Reference 81.
[d]Reference 82.
[e]Reference 1.

calculated to be 1.15×10^{-9} m^2 s^{-1} [experimentally, 2.3×10^{-9} m^2 s^{-1} at 298 K]. This value is low compared to the experimental value at 298 K, but agrees with an experimental value of 1.17×10^{-9} m^2 s^{-1} for a water temperature of 275 K.[73] Hence, although the calculated diffusion coefficient is too low for the simulation temperature of 300 K, it still falls within the range for liquid water.

Other results from the MD simulation which can be verified against experimental data are the radial distribution functions (RDF's) of the various ions in the system. Figure 3 shows the RDF's for the O-O, O-H, and H-H pairs, where the peaks due to intramolecular interactions have been omitted. The RDF between oxygen atoms shows a very clear

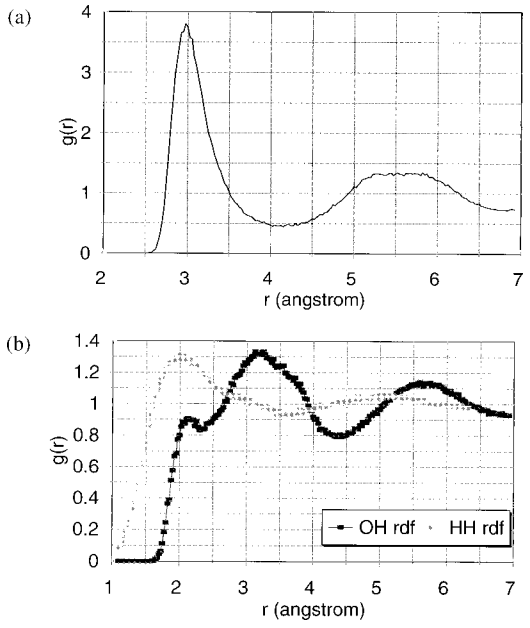

FIG. 3. (a) O-O and (b) O-H and H-H radial distribution functions, omitting intramolecular OH and HH interactions.

TABLE III. Calculated and experimental properties of liquid water.

Property	Properties of liquid water NPT	Experiment
G_{OO}/Å (Height)	2.97 (3.80)	2.88 (3.10)
$\langle E_i\rangle$/kJ mol^{-1}	−42.7	−41.7
ρ/g cm^{-3}	1.30	0.997
C/J mol^{-1} K^{-1}	98.2	75.6
κ/Mbar^{-1}	37.1	45.7
$D/10^{-9}$ m^2 s^{-1}	1.15	2.30

peak at 2.97 Å and a broader area between 5 and 6 Å. The first peak is in good agreement with experimental findings (2.88 Å),[74] although the experimental value for the second peak at 4.6 Å (Ref. 75) is somewhat smaller than the calculated value, though in line with other water potential models (cf. 5.4 Å for a flexible TIPS model).[76] The heights of the peaks, 3.8 and 1.3, compare well to experimental values of 3.1 and 1.1,[74] indicating that our model shows ordering of the water molecules which agrees adequately with experimental findings. The first peak of the O-H RDF at 2.12 Å is again at a somewhat larger distance than that found experimentally (1.9 Å), although the second maximum at 3.13 Å agrees very well with experimentally observed RDF's (3.2 Å). The heights of the peaks of 0.9 and 1.3 compare favorably with experimental values of 1.0 and 1.3.[74] Finally, the H-H RDF shows a peak at 2.6 Å of height 1.3, a shoulder at about 3.5 Å (height±1.0) and another peak at 5.7 Å of height 1.1. This compares with experimental peaks at 2.3, 3.7 and 4.9 Å, heights 1.3, 1.2 and 1.0 respectively, which again is in good agreement.[74] Overall, the simulated and experimental systems show similar ordering of the water molecules.

As we were interested in obtaining hydration energies for the adsorption of water molecules onto solid surfaces, a good test of our potential model would be to obtain an energy of vaporization from our MD simulations. We calculated this vaporization energy from the interaction energies between the water molecules in the system. The energy of vaporization hence calculated is 43.0 kJ mol^{-1}, which is in excellent agreement with the experimental value of 43.4 kJ mol^{-1} at 310 K.[11]

Table III compares additional data obtained from the MD simulations using our shell potential model with experiment.[24] It is clear that the shell model does not reproduce the experimental density or self-diffusion coefficient accurately. However, when the density is kept fixed at the experimental density of approximately 1 g cm^{-3} in a NVT simulation, which is the ensemble usually applied when modeling liquid water, the diffusion coefficient obtained is 3.5×10^{-9} m^2 s^{-1}. This is in better agreement than some previous potential models, such as the CVFF and rigid SPC and TIP models, where diffusion coefficients range from 4.2 to 6.7×10^{-9} m^2 s^{-1}, and comparable to more sophisticated models such as the flexible SPC model [$D=(3.1-3.6)\times10^{-9}$ m^2 s^{-1}].[24] The high density from our model may be due to the fact that the geometry of our calculated water dimer as mentioned above does not agree with the experimentally found structure. The angle θ_a (Fig. 1) at 30.1° is

smaller by at least 16° than its experimental counterpart ($57 \pm 10°$), which makes the calculated dimer too flat. This may encourage the formation of a layered structure, and these layers would be able to approach more closely, increasing the density at fixed pressure.

Despite the above shortcomings of the shell-model water potential, we feel that its compatibility with the interatomic potentials for polar solids and its agreement with experimental parameters (geometry of monomer and dimer, dipole moment, dimer binding energy, radial distribution functions, average intermolecular energy $\langle E_i \rangle$, and vaporization energy) make it a valid model to study interactions between oxide surfaces and water, and, hence, in the next subsection we describe the results of molecular-dynamics simulations of two MgO surfaces in liquid water using the shell model water potential.

MgO surfaces in liquid water

We studied two MgO surfaces, the {100} surface, which is the most stable and dominant surface and is known to react rapidly with water,[77,78] and the {310} surface, which is a good model for the experimental {100} surface including monatomic steps.[78] Using the DL_POLY program,[62] we performed several MD simulations, both *in vacuo* as an NVT ensemble and in a system of liquid water which made it possible to run under NPT conditions. Thus we can investigate whether the stability of the surfaces may be influenced by the mobility of the water molecules. All MD simulations were performed at 300 K for a simulation time of 150 ps.

{*100*} *surface*

The simulation cell for the {100} surface consisted of a MgO $4\times4\times4$ supercell containing 256 MgO units consisting of cores and shells on the oxygen atoms. The gap between the surfaces of the repeated cell was 30 Å, containing 275 water molecules, the whole system consisting of 1868 species including shells. The average surface energy of the unhydrated {100} surface obtained from the NVT simulations *in vacuo* was calculated to be 1.31 J m^{-2} at 300 K, comparable to that obtained from previous static calculations (1.25 J m^{-2}).[77] After running the MgO slabs with the water molecules under NPT conditions, the average surface energy was calculated to be 2.89 J m^{-2}, indicating that the {100} surface in liquid water is not very stable. This is further confirmed by the average hydration energy of $+28.5$ kJ mol^{-1}, which shows that hydration of the {100} under liquid water conditions is an endothermic process.

The RDF's between magnesium ions and the oxygen atoms of the water molecules, and between surface lattice oxygen ions and hydrogen atoms, are shown in Fig. 4. The first peaks at 2.0 and 1.8 Å, respectively, are in accord with the experimentally found Mg-O_{water} distances in hydrated magnesium salts[79] and hydrogen-bonding.[80] The self-diffusion coefficient of the water molecules between the slabs of MgO was calculated to be 4.7×10^{-9} m^2 s^{-1}, a large increase from the value of 1.15×10^{-9} m^2 s^{-1} for the system of pure water. This is probably due to the fact that the density of the water molecules between the slabs has decreased from the pure water value of 1.3 to 1.00 g cm^{-3} between the MgO surfaces. As such, the water molecules have scope to move more

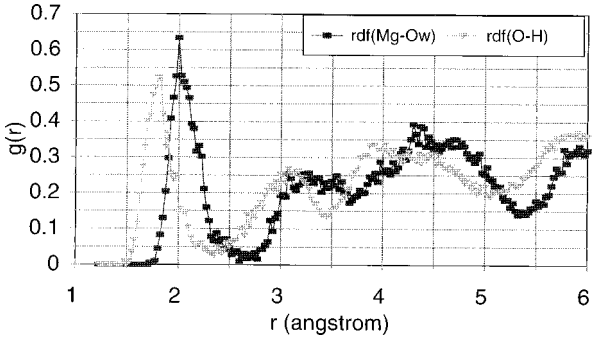

FIG. 4. Mg-O_{water} and $O_{lattice}$-H radial distribution functions of the NPT simulation of the MgO {100} surface in water at 300 K.

freely. The decrease in density may imply that the water is repelled by the MgO surfaces or at least that the MgO surface disrupts the hydrogen bonding in the water. However, when we look at a histogram of the number of water molecules as a function of distance from the MgO slab (Fig. 5), it is clear that the water density is greatest near the MgO surface, and that there is a clear preferred orientation on the surface. This disrupts the bonding with the next layer of water, and hence the density decreases in the next few layers toward a fairly level density midway between the two slabs. Together with the lower density, the implication is that the adsorption pattern on the surface forces the water molecules in subsequent layers to form an intermolecular configuration which is more open than in the system of pure water. Although rather more speculative, the oscillatory behavior in the density (Fig. 5), with two low-density areas at 9–10 Å from the slab surfaces, may indicate an even longer range disruption of the bulk water structure than just the monolayer adsorbed on the surfaces. Of course, this effect may have been exacerbated by the relatively small number of water molecules in the system. It would therefore be interesting to model a larger system containing more water molecules, but at present, due to the use of shell-model potentials, the system modeled here is stretching computational resources to the limit.

The hydration energy was calculated and as shown in Table IV the energy is positive. In order to investigate

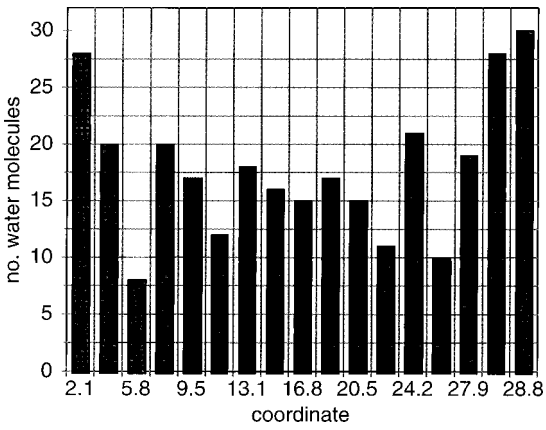

FIG. 5. Histogram of the water molecules between the slabs of MgO {100} showing the average number of water molecules as a function of the position coordinate normal to the surface, where the two {100} surfaces are at 0 and 31 Å.

TABLE IV. Data obtained from MD simulations of MgO {100} and {310} surfaces in water at 300 K.

Surface	Simulation	$\langle\rho\rangle$/ g cm^{-3}	$\langle D\rangle/10^{-9}$ m^2 s^{-1}	$\langle E_{hydr}\rangle$/ kJ mol^{-1}	$\langle\gamma\rangle$/ J m^{-2}
{100}	NPT	1.00	4.70	+28.5	2.89
	NVT	0.23	16.70	+6.8	1.43
{310}	NPT	0.93	6.10	+18.7	2.74
	NVT	0.31	15.4	−15.1	1.25

whether the unstable hydration and surface energies are dependent on the density of the water surrounding the slab, we performed further simulations at a water density of 0.23 g cm^{-3}, which corresponds to a sufficient number of water molecules to cover the surface with a full monolayer. We collected data at different times during the simulation to monitor any changes in properties, such as the self-diffusion coefficient. The results are collected in Table IV. Calculating the average hydration energy and average surface energy at different intervals during the NVT simulation (20, 100, and 150 ps), they showed that the system had settled after approximately 100 ps, and no further significant changes in hydration energy (+5.3 kJ mol^{-1} after 100 ps and +6.8 kJ mol^{-1} after 150 ps) and surface energy (+1.40 J m^{-2} after 100 ps and +1.43 J m^{-2} after 150 ps) were observed. The self-diffusion coefficient was calculated at the same intervals, and was seen to decrease from an initial value of 36.7 $\times 10^{-9}$ m^2 s^{-1} after 20 ps, to 18.1$\times 10^{-9}$ m^2 s^{-1} after 100 ps, which then remained relatively stable and settled at 16.7$\times 10^{-9}$ m^2 s^{-1} after 150 ps. The system had stabilized to a slab of MgO with a monolayer of adsorbed water molecules on the surfaces which are immobile apart from vibrations around their adsorbed position. Two snapshots of the MgO {100} slab after 100 and 150 ps are shown in Fig. 6, from which it is clear that no significant changes have taken place in the final 50 ps. Any water molecules not in the first adsorbed layer do not form a second layer, but move away from the surface and move randomly through the low-density gap between the slabs. The higher self-diffusion coefficient in the NVT system than in the denser NPT simulation is probably due to this more open water structure above the first adsorbed water layer, leading to fewer attractive interactions between the water molecules.

The MgO surface which was fully covered in the NPT simulation is now only partially hydrated to a coverage of approximately 78%, in agreement with previous static calculation[78] which showed a partial coverage of 75% to be particularly stable. Figure 6 shows that the water molecules adsorb in a flat configuration, coordinating to the magnesium atom by their oxygen atoms, and hydrogen bonding to two lattice oxygen atoms. A pattern of adsorption is developing where the water molecules adsorb in diagonal rows across the surface, which alternate in a herringbone pattern in the direction in which the hydrogen atoms are pointing. It would seem, though, that the water molecules are too large to adsorb completely flat in this fashion, and that each molecule is rotated somewhat with respect to its neighbor. Vacancies occur where hydrogen atoms of neighboring adsorbed molecules come too close to each other. This pattern of adsorption disrupts the structure of the water in the vicinity of the surface, especially as a second layer (not shown) prefers not to be adsorbed on top of the first explaining the sharp drop in water density away from the surface (Fig. 5). This absence of an ordered structure between the first and subsequent water layers is observed experimentally by infrared visible SFG spectroscopy at neutral quartz/water interfaces,[31] where at low pH when the quartz surface is uncharged, comparable to our MgO surfaces, the water molecules adsorb with their oxygen atoms toward the surface but without particular orienting of water layers further away from the surface. Only with charged quartz surfaces (at high pH), when the water molecules adsorb by hydrogen bonding to the surface, is the surface field found to align 3–5 layers of water molecules.[31] The high positive value for the average hydration energy of the NPT simulation is thus probably due to the intermolecular interactions between adsorbed water molecules and subsequent layers which are disrupted from preferred configurations, rather than the interactions between adsorbed water molecules and the surface. This also explains why previous

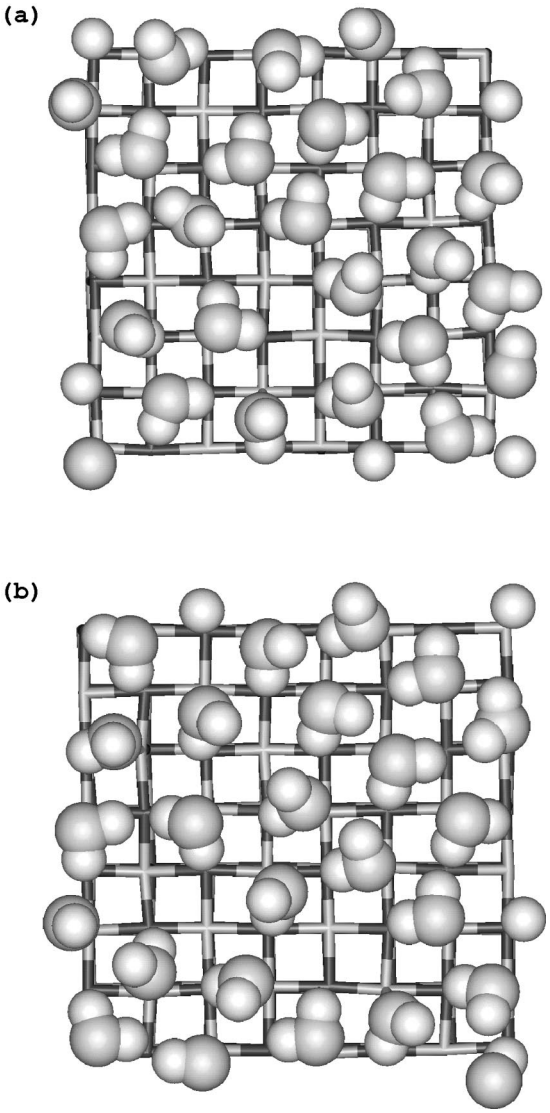

FIG. 6. Snapshots of water adsorption on the MgO {100} surface at 300 K and NVT, $\rho = 0.23$ g cm^{-3}, after (a) 100 ps and (b) 150 ps. MgO is shown as the framework structure (Mg, pale grey; $O_{lattice}$, dark gray; O_{water}, light gray; H, white).

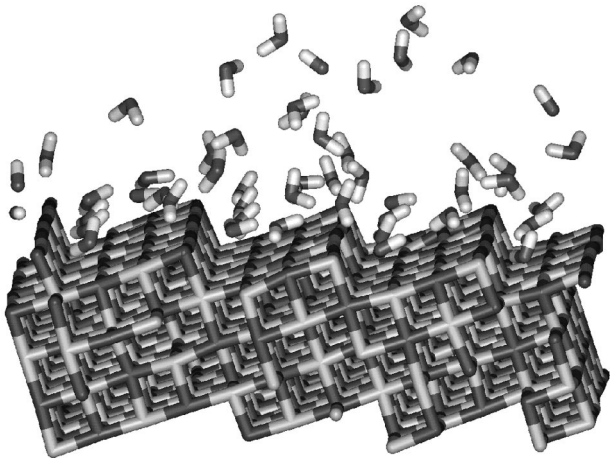

FIG. 7. Snapshot of the MgO {310} surface with adsorbed water molecules after 150 ps, at 300 K and $\rho = 0.31$ g cm^{-3}, showing regular adsorption of the water molecules' oxygen atoms to both edge and plane magnesium ions. MgO is shown as the framework structure (Mg, pale gray; O, dark gray; H, white).

static simulations,[78] and other calculations[48,51] which only modeled single layers of adsorbed water molecules, found adsorption, notably at partial coverages, to be an exothermic process, especially as gaseous water was considered which would lower the hydration energies compared to liquid water by 43.0 kJ mol^{-1}.

{*310*} *surface*

The {310} surface gave similar results to the {100} surface above. This system consisted of 384 MgO units with 327 water molecules in a gap of 25 Å, the whole system comprising 2460 species including shells. The RDF between magnesium ions and the water molecules' oxygen atoms has its first peak at the somewhat larger value of 2.1 Å. This is explained by the adsorption behavior of the water molecules, which ''prefer'' to adsorb with their oxygen atom in the interstitial lattice oxygen site on the edge, doubly coordinated to magnesium ions on both the edge and the plane below (Fig. 7). The negative hydration energy of the NVT simulation indicates that this mode of adsorption is particularly favorable, in agreement with previous static calculations.[78] Figure 7 shows a definite pattern of adsorption at those sites, but no formal pattern on the remainder of the {100} planes making up the stepped {310} surface, even though the NVT system was fully stabilized and showed no significant changes in either self-diffusion coefficient or average surface and hydration energies after 20 ps. Rather, the water molecules tend to drift away from the surface, which again shows that {100} planes prefer not to be fully hydrated, also indicated by the positive hydration energy of the NPT simulation.

IV. CONCLUSION

From the above results we can make the following observations.

(i) The shell-model water potential models the water monomer and dimer well, and reproduces structure and binding energy.

(ii) The density of simulated liquid water at constant pressure and temperature is too large, possibly due to the absence of directional hydrogen-bonding. This results in the self-diffusion coefficient being too small, although still in the region of liquid water.

(iii) The ordering of the simulated liquid water, observed from the various RDF's, is in good agreement with experiment, as are the energy of vaporization, the average energy, the specific-heat capacity, and the compressibility.

(iv) When modeling the {100} and {310} surfaces of MgO in liquid water under NPT conditions, the density is decreased, indicating disruption of the water structure. The adsorption pattern at the surfaces and the density profile of the water normal to the surface indicates that this is due to the energetically unfavorable interactions between adsorbed molecules and subsequent water layers. NVT simulations at lower water densities indicate that adsorption at interstitial lattice sites on the {310} surface are energetically favorable, while hydration at the {100} is still just endothermic, probably due to the imperfect matching of the water molecules to the MgO lattice.

(v) These simulations have shown that molecular-dynamics simulations can give insight into adsorption behavior and solvent effects which may not be accessible with simple static atomistic simulation techniques.

From the results above we believe that the shell-model water potential, developed as a transferable potential compatible with available potential models for inorganic solids, is suitable for the study of hydration of those solids or as a solvent in more complex simulations.

ACKNOWLEDGMENTS

We thank EPSRC and NERC for financial support, the Materials Consortium for computer time on the T3D, and Molecular Simulations Inc. for the provision of Insight II.

*Electronic address: n.h.deleeuw@bath.ac.uk
†Electronic address: s.c.parker@bath.ac.uk

[1] T. R. Dyke, K. M. Mack, and J. S. Muenter, J. Chem. Phys. **66**, 498 (1977).
[2] J. E. Bertie, M. K. Ahmed, and H. H. Eysel, J. Phys. Chem. **93**, 2210 (1989).
[3] Y. Marechal, J. Phys. Chem. **97**, 2846 (1993).
[4] J. P. Devlin and V. Buch, J. Phys. Chem. **99**, 16 534 (1995).
[5] A. F. Bunkin, G. A. Lyakhov, A. A. Nurmatov, and A. V. Rezov, Phys. Rev. B **52**, 9360 (1995).
[6] J. Huang and L. S. Bartell, J. Phys. Chem. **99**, 3924 (1995).
[7] F. Bruni, M. A. Ricci, and A. K. Soper, Phys. Rev. B **54**, 11 876 (1996).
[8] J. Brodtholt and B. Wood, J. Geophys. Res. **98**, 519 (1993).
[9] S. Goldman and C. Joslin, J. Phys. Chem. **97**, 12 349 (1993).
[10] I. M. Svishchev and P. G. Kusalik, J. Phys. Chem. **98**, 728 (1994).
[11] Z. Duan, N. Moller, and J. H. Weare, Geochim. Cosmochim. Acta **59**, 3273 (1995).
[12] I. M. Svishchev and P. G. Kusalik, J. Am. Chem. Soc. **118**, 649 (1996).
[13] M. I. Heggie, C. D. Latham, S. C. P. Maynard, and R. Jones,

Chem. Phys. Lett. **249**, 485 (1996).
[14] G. Ruocco, F. Sette, M. Krisch, U. Bergmann, C. Masciovecchio, and R. Verbeni, Phys. Rev. B **54**, 14 892 (1996).
[15] P. Johansson, Phys. Rev. B **54**, 2988 (1996).
[16] F. Franks, *The Physics and Physical Chemistry of Water* (Plenum, London, 1976).
[17] B. Kamb, in *Water and Aqueous Solutions*, edited by R. A. Horne (Wiley, New York, 1972).
[18] A. Wallqvist and B. J. Berne, J. Phys. Chem. **97**, 13 841 (1993).
[19] W. L. Jorgensen, J. Am. Chem. Soc. **103**, 335 (1981).
[20] W. L. Jorgensen, J. Am. Chem. Soc. **77**, 4156 (1982).
[21] W. L. Jorgensen, J. Chandrasekhar, J. D. Madura, R. W. Impey, and M. L. Klein, J. Chem. Phys. **79**, 926 (1983).
[22] A. D. Trokhymchuk, M. F. Holovko, and K. Heinzinger, J. Chem. Phys. **99**, 2964 (1993).
[23] D. N. Bernardo, Y. Ding, K. Krogh-Jespersen, and R. M. Levy, J. Phys. Chem. **98**, 4180 (1994).
[24] K. F. Lau, H. E. Alper, T. S. Thacher, and T. R. Stouch, J. Phys. Chem. **98**, 8785 (1994).
[25] S. W. Rick, S. J. Stuart, and B. J. Berne, J. Chem. Phys. **101**, 6141 (1994).
[26] S.-B. Zhu and C. F. Wong, J. Phys. Chem. **98**, 4695 (1994).
[27] J. Brodtholt, M. Sampoli, and R. Vallauri, Mol. Phys. **85**, 81 (1995).
[28] J. Brodtholt, M. Sampoli, and R. Vallauri, Mol. Phys. **86**, 149 (1995).
[29] B. G. Dick and A. W. Overhauser, Phys. Rev. B **112**, 90 (1958).
[30] J. D. Porter and A. S. Zinn, J. Phys. Chem. **97**, 1190 (1993).
[31] Q. Du, E. Freysz, and Y. R. Shen, Phys. Rev. Lett. **72**, 238 (1994).
[32] D. A. Rose and I. Benjamin, J. Chem. Phys. **100**, 3545 (1994).
[33] A. Delville and M. Letellier, Langmuir **11**, 1361 (1995).
[34] A. B. Horn, S. F. Banham, and M. R. S. McCoustra, J. Chem. Soc., Faraday Trans. **91**, 4005 (1995).
[35] M. I. McCarthy, G. K. Schenter, M. R. Chacon-Taylor, J. J. Rehr, and G. E. Brown Jr., Phys. Rev. B **56**, 9925 (1997).
[36] W. Langel and M. Parrinello, Phys. Rev. Lett. **73**, 504 (1994).
[37] M.-C. Wu, C. A. Estrada, J. L. Corneille, and D. W. Goodman, J. Chem. Phys. **96**, 3892 (1992).
[38] C. Li, G. Li, and Q. Xin, J. Phys. Chem. **98**, 1933 (1994).
[39] H. Dunski, W. K. Jozwiak, and H. Sugier, J. Catal. **146**, 166 (1994).
[40] S. Coluccia, A. J. Tench, and R. L. Segall, J. Chem. Soc., Faraday Trans. 1 **75**, 1769 (1979).
[41] S. Coluccia, A. Barton, and A. J. Tench, J. Chem. Soc., Faraday Trans. 1 **77**, 2203 (1981).
[42] C. F. Jones, R. A. Reeve, R. Rigg, R. L. Segall, R. St. C. Smart, and P. S. Turner, J. Chem. Soc., Faraday Trans. 1 **80**, 2609 (1984).
[43] H. Onishi, C. Egawa, T. Aruga, and Y. Iwasawa, Surf. Sci. **191**, 479 (1987).
[44] C. Duriez, C. Chapon, C. R. Henry, and J. M. Richard, Surf. Sci. **230**, 123 (1990).
[45] C. A. Scamehorn, A. C. Hess, and M. I. McCarthy, J. Chem. Phys. **99**, 2786 (1993).
[46] S. Picaud, P. N. M. Hoang, and C. Girardet, Surf. Sci. **278**, 339 (1992).
[47] C. Noguera, J. Goniakowski, and S. Bouette-Russo, Surf. Sci. **287/288**, 188 (1993).
[48] C. A. Scamehorn, N. M. Harrison, and M. I. McCarthy, J. Chem. Phys. **101**, 2786 (1994).
[49] W. Langel and M. Parrinello, J. Chem. Phys. **103**, 337 (1995).
[50] J. Goniakowski and C. Noguera, Surf. Sci. **330**, 337 (1995).
[51] K. Refson, R. A. Wogelius, D. G. Fraser, M. C. Payne, M. H. Lee, and V. Milman, Phys. Rev. B **52**, 10 823 (1995).
[52] M. Born and K. Huang, *Dynamical Theory of Crystal Lattices* (Oxford University Press, Oxford, 1954).
[53] P. P. Ewald, Ann. Phys. (Leipzig) **64**, 253 (1921).
[54] D. E. Parry, Surf. Sci. **49**, 433 (1975).
[55] D. E. Parry, Surf. Sci. **54**, 195 (1976).
[56] J. H. Harding, Rep. Prog. Phys. **53**, 1403 (1990).
[57] C. R. A. Catlow and W. C. Mackrodt, *Computer Simulation of Solids* (Springer-Verlag, Berlin, 1982).
[58] P. S. Baram and S. C. Parker, Philos. Mag. B **73**, 49 (1996).
[59] J. D. Gale, J. Chem. Soc., Faraday Trans. **93**, 629 (1997).
[60] G. V. Lewis and C. R. A. Catlow, J. Phys. C **18**, 1149 (1985).
[61] K. P. Schroder, J. Sauer, M. Leslie, C. R. A. Catlow, and J. M. Thomas, Chem. Phys. Lett. **188**, 320 (1992).
[62] T. R. Forester and W. Smith, *DL_POLY User Manual* (CCLRC, Daresbury Laboratory, Warrington, UK, 1995).
[63] L. Verlet, Phys. Rev. **159**, 98 (1967).
[64] S. Nosé, J. Chem. Phys. **81**, 511 (1984).
[65] W. G. Hoover, Phys. Rev. A **31**, 1695 (1985).
[66] P. J. D. Lindman and M. J. Gillan, J. Phys.: Condens. Matter **5**, 1019 (1993).
[67] P. J. Mitchell and D. Fincham, J. Phys.: Condens. Matter **5**, 1031 (1993).
[68] R. Ferneyhough, D. Fincham, G. D. Price, and M. J. Gillan, Modell. Simul. Mater. Sci. Eng. **2**, 1101 (1994).
[69] D. Eisenberg and W. Kauzmann, *The Structure and Properties of Water* (Oxford University Press, Oxford, 1969).
[70] S. C. Parker, and G. D. Price, Adv. Solid State Chem. **1**, 295 (1989).
[71] B. Kamb, Trans. Am. Crystallogr. Assoc. **5**, 61 (1969).
[72] M. P. Allen and D. J. Tildesley, *Computer Simulation of Liquids* (Oxford University Press, Oxford, 1993).
[73] K. Krynicki, C. D. Green, and D. W. Sawyer, Faraday Discuss. Chem. Soc. **66**, 199 (1978).
[74] A. K. Soper and M. G. Phillips, Chem. Phys. **107**, 47 (1986).
[75] A. H. Narten and H. A. Levy, J. Chem. Phys. **55**, 2263 (1971).
[76] L. X. Dang and B. M. Pettitt, J. Phys. Chem. **91**, 3349 (1987).
[77] N. H. de Leeuw, G. W. Watson, and S. C. Parker, J. Phys. Chem. **99**, 17 219 (1995).
[78] N. H. de Leeuw, G. W. Watson, and S. C. Parker, J. Chem. Soc., Faraday Trans. **92**, 2081 (1996).
[79] R. T. Forbes, P. York, V. Fawcett, and L. Shields, Pharmaceut. Res. **9**, 1428 (1992).
[80] N. T. Skipper, A. K. Soper, and M. V. Smalley, J. Phys. Chem. **98**, 942 (1994).
[81] J. A. Odutola and T. R. Dyke, J. Chem. Phys. **72**, 5062 (1980).
[82] L. A. Curtiss, D. J. Frurip, and M. Blander, J. Chem. Phys. **71**, 2703 (1979).